Liquid-liquid interface microchannels with tunable mechanical properties mimic tissue deformations during neutrophil interstitial migration *in vivo*

Jonathan Schrope[1, 2, 3, 4], Adam Horn[2], Mehtab Farooqui[3], Grace Li[1, 2], Adeel Ahmed[5], Terry Juang[1, 3], Chao Li[5, *], Anna Huttenlocher[2, 6, *], David Beebe[1, 2, 3, 5, *]

[1]Department of Biomedical Engineering, University of Wisconsin-Madison, Madison, WI, USA

[2]Department of Medical Microbiology and Immunology, University of Wisconsin-Madison, Madison, WI, USA

[3]Department of Pathology, University of Wisconsin-Madison, Madison, WI, USA

[4]Medical Scientist Training Program, University of Wisconsin-Madison, Madison, WI, USA

[5]Carbone Cancer Center, University of Wisconsin-Madison, Madison, WI, USA

[6]Department of Pediatrics, University of Wisconsin-Madison, Madison, WI, USA

* Co-corresponding authors

ABSTRACT

Cell migration plays an essential role in the immune response and is tightly regulated by both chemical and mechanical cues. After exiting circulation, immune cells navigate through tissues while mechanically confined by extracellular matrix components and tissue-resident cells. Common *in vitro* systems enable modeling of leukocyte migration through collagen-based hydrogels (individual fiber stiffness ~ 300 MPa) or in confined polymer-based microchannels (stiffness > MPa), however these existing systems fail to replicate the bidirectional mechanical interactions between migrating leukocytes and resident cells that typically exhibit a stiffness between 200-3000 Pa. Here, we utilize live-imaging of a dual-transgenic zebrafish to capture mechanical deformations of epidermal keratinocytes induced by interaction with migrating neutrophils. Subsequently, we engineer *in vitro* migration channels bound by a deformable liquid-liquid interface with tunable mechanical properties that replicate single cell keratinocyte deformations during neutrophil migration *in vivo*. We find that controlling the mechanical properties of the interface modulates neutrophil motility. This work introduces an *in vitro* controlled material interface that closely mimics the mechanical interactions between neutrophils and surrounding cells *in vivo* to provide a biologically relevant platform for exploring the influence of mechanical forces on cell migration.

INTRODUCTION

Precise regulation of leukocyte migration to sites of infection, malignancy, and injury is required for successful mounting and resolution of the immune response. This process is tightly regulated i*n vivo* by a combination of chemical gradients and local mechanical cues. For example, cells migrate through tissues confined by surrounding extracellular matrix (80% collagen by mass) but also tissue-resident cells that make up the majority of tissue volume (*1-3*). The ability for rapid cytoskeletal reorganization allows leukocytes to exert substantial amounts of mechanical force to deform surrounding cells, which in turn mechanically confine migrating leukocytes. This bi-directional mechano-reciprocity between leukocytes and tissue-resident cells regulates levels of immune cell activation as well as migration speed and directionality (*3*). Neutrophils are the most abundant and motile cells in the immune system, and therefore it is important to understand how local mechanical cues regulate trafficking to sites of infection or injury (*3,4*).

While *in vivo* models provide a complexity of physical cues during neutrophil migration to sites of infection (*5,6*) or wounds (*7, 8*), they do not allow precise control over local mechanical properties. Hence, the use of *in vitro* models to study leukocyte migration has proven integral in dissecting how physical interactions with the environment drive cell phenotype. For example, the development of hydrogels with tunable stiffness and pore size has enabled the study of how mechanical reciprocity of cell-matrix interactions modulates migration speed and directionality (*9, 10*). However, such systems are only tunable to an average pore size or bulk stiffness (100 - 2000 Pa), with limited

control over the mechanical properties of individual collagen fibers that confine migrating neutrophils (stiffness ~300 MPa (*11*)).

To allow for more precise control over mechanical properties sensed by individual leukocytes, alternative approaches utilize polymeric materials such as polyacrylamide (bulk stiffness ~ 10-1000 kPa (*12*)), agarose (stiffness ~ kPa (*13*)), or polydimethylsiloxane (PDMS) based microchannels (stiffness ~ 800 kPa - 10 MPa (14)) to study how controlled confinement of individual cells modulates traction (15), polarity (*16,17*), migration direction, speed (*18-21*), and cell-cell communication (*22-23*). However, the use of materials orders of magnitude higher than the stiffness of resident cells (most single cells ~200-3000 Pa (11)) prevents modeling of the mechanical interactions between immune cells and surrounding cells *in vivo*. This poses a challenge to engineer an *in vitro* material with comparable mechanical properties to individual cells to provide a confining yet deformable interface for migrating leukocytes to navigate *in vitro*.

Here, we utilize live-imaging of a dual-transgenic zebrafish model to characterize the mechanical interactions between migrating neutrophils and surrounding keratinocytes *in vivo*. To model similar mechanical interactions *in vitro*, we developed microchannels of a deformable liquid-liquid interface to study neutrophil migration along a collagen substrate confined by single-cell scale forces provided by the interfacial tension of an oil-media interface. Confinement forces are governed by droplet capillary pressure and thus tunable within the range of many cell types (200-600 Pa initial channel capillary pressures

and 200-3000 Pa local equilibrium pressures resisting cell deformation). We find that neutrophil migration speed is dependent on the degree of required interfacial deformation and the interfacial pressure resisting deformation. Thus, neutrophils that reach the deformable interface first (pioneer cells) require greater deformation of the interface than trailing cells and as a result migrate slower. Furthermore, tuning the mechanical properties of the interface modulates migration speed and replicates the mechanical deformations of surrounding keratinocytes observed *in vivo*. This work introduces a tunable material interface that replicates individual cell-scale forces to study how local mechanical cues provided by a soft interface modulate leukocyte motility.

RESULTS

Neutrophils deform surrounding keratinocytes during homeostatic migration in zebrafish.

After exiting the circulation, neutrophils navigate through tissues of varying mechanical properties. Zebrafish have emerged as a leading *in vivo* model to study leukocyte morphology and migration due to its transparency and high optical clarity (24). To image the interactions between neutrophils and epithelial cells during interstitial migration, we used dual transgenic larval zebrafish (*Tg(mpx:mCherry) x Tg(Krtt1c19e-acGFP))* that express mCherry in neutrophils and GFP in basal keratinocytes. The basal keratinocytes form a single layer of cells in the epidermis at 3 days post-fertilization (dpf) (**Fig 1A**). Time-

lapse imaging of the skin above the yolk sac shows the typical morphologies of motile neutrophils in zebrafish with dynamic pseudopod formation (**Fig 1B**). Dual imaging reveals that neutrophils often migrate in spaces between basal epithelial cells in this region of the zebrafish (**Fig 1C**). Migrating neutrophils deform surrounding keratinocytes during this migration (**Fig 1D**) and these deformations are elastic in nature (**Fig 1E**). These data demonstrate that neutrophils are mechanically confined by and dynamically interact with surrounding basal epithelial cells as they navigate through tissues.

Construction of collagen coated liquid-liquid microchannels on single-cell length scales.

In comparison to *in vivo* models, the control afforded by *in vitro* systems has proven essential to understanding how local physical cues alter leukocyte phenotype. However, while many *in vitro* systems examine leukocyte response to physical constraints during migration through hydrogels or confined microchannels, existing systems fail to replicate mechanical interactions with a soft, deformable interface like that of surrounding cells. To construct a platform to study neutrophil interaction with a deformable interface, we leverage a recent discovery of exclusively liquid repellent (ELR) surfaces (*23, 24*) to construct microchannels made of a liquid-liquid interface on length scales comparable to single cells (2-10 µm) [2020 Sci Adv].

Alternative methods have engineered liquid-walled microchannels by printing of aqueous media onto substrates (*25, 26, 27*) or selective patterning of superhydrophobic-

hydrophilic regions (*28*). However, the construction of channels with heights on single-cell length scales to examine interface interaction with cells requires the engineering of exclusively liquid-repellent surfaces (*29*), that is a surface that completely repels aqueous media. The degree to which a solid surface repels a liquid within a three-phase system (ex. solid-liquid-liquid) is reflected in the Young's contact angle (θ) that the liquid droplet makes on the surface. The Young's contact angle is determined by the precise balance between all interfacial energies (γ_{SL1}, γ_{SL2}, γ_{L1L2}) present within the system. Careful engineering of this energy balance can result in a surface completely repellent to a liquid, characterized by a Young's contact angle of 180° (**Fig 2A**).

Here, we chemically pattern a glass surface (e.g., standard microscopic glass slide, cover glass) to exhibit a double ELR system; complete repellency of aqueous solution in some areas (Water Repellent Surface, WRS) and oil in others (Oil Repellent Surface, ORS) (**Fig 2B**). Media deposited onto the patterned surface by "sweeping" a hanging drop with a pipette is pinned to ORS areas due to complete repulsion by WRS areas (**Fig 2C**). The result is two droplets with a connecting liquid channel (**Fig 2D**). A representative channel of 30 µm width has a height of ~ 2 µm (**Fig 2E**). Channel height is controlled by channel width, constrained by the patterning process (**Supplementary Fig 1**).

While collagen is the most abundant ECM protein in the body and provides significant physical (*3, 30, 31, 32*) and chemical (*33*) cues to migrating cells, its high viscosity and rapid polymerization rate limits incorporation into traditional closed

microchannels on sub-10 µm length scales. Existing methods utilize external pumping of collagen into closed channels (*34, 35*), decreasing throughput and increasing adoption barrier. Here, channels are constructed in open fluid, allowing for direct physical access so that performing the sweep technique with neutralized collagen yields microchannels on single cell length scales made of fibrillar collagen (**Fig 2F and G**).

The interfacial pressure of liquid-liquid microchannels confines neutrophils with an interface of similar properties as tissue-resident cells

To investigate neutrophil interaction with the liquid-liquid interface of this system, channels were constructed by sweeping a solution of cells suspended in neutralized collagen (**Fig 3A**). Cells placed in channels of sequentially decreasing size (200 µm to 30 µm channel widths) exhibit decreasing cell height, implicating sufficient interfacial rigidity to mechanically confine single cells (**Fig 3B**). However, differences in interfacial height between locations with and without cells show that the interface is not a rigid barrier such as plastic or PDMS elastomer but deformable by the presence cells (**Fig 3C**). Thus, the interface provides forces comparable to single neutrophil stiffness to both confine yet deform in response to the presence of a cell. The pressure resisting cell deformation is the capillary pressure which arises from the presence of curvature across the interface. Thus, pressure is a function of the interfacial energy between the oil and aqueous media phase (γ_{OM} = 41.8 mN/m for DI water and silicone oil (*23*)) and the radii of curvature of the interface (**Fig 3D**). The channel alone exhibits curvature only along the channel width (infinite curvature along length), whereas the presence of cells generates local curvature

along the length and width of the cell (**Fig 3E**). The result is an initial pressure that cells must overcome to deform the interface and an equilibrium pressure that resists further deformation and governs final cell height. Both channel and equilibrium pressures decrease with increasing channel width. Additionally, initial channel height is a function of channel width and determines the point at which cells will contact the interface (**Fig 3F**). The result is a dependence of cell heights on the balance between cell stiffness, pressure resisting deformation, and initial channel height. Cell height thus increases with channel width (**Fig 3E**), demonstrating the ability to control the confinement of cells to different degrees within microchannels of a liquid-liquid interface.

A liquid-liquid interface enables open fluid cell trapping and gradient formation along a collagen substrate

As neutrophils mechanically interact with tissue-resident cells, chemical cues arising from sites of injury or infection influence migration path and speed. The generation of chemokine gradients to study cell migration within *in vitro* systems requires physical separation of cells from chemical cues (*36*), traditionally accomplished by patterning cells in space with rigid PDMS walls (*37*, *38*). Furthermore, controlling cell exposure to varying amounts of a chemical requires precise positioning of cells within an established gradient. Given the findings that a liquid-liquid interface possesses a rigidity sufficient to confine cells, we hypothesized that this interface could act as a physical barrier to allow spatial trapping of cells at the channel entrance.

To examine this, channels were constructed with collagen, followed by sequential addition of cells to the inlet droplet by pipetting. The result is a layer of media containing cells upon a layer of collagen fibers (**Fig 4A**). A representative profile of the media and collagen layers is shown in **Fig 4B** for a 200 µm width channel. Notably, the height of the media layer decays to zero at some point along the length of the channel (~ 130 µm for a 200 µm width channel). If the oil-media interface possesses a rigidity to spatially trap cells, then the height of the media layer controls cell positioning along the entrance to the channel. We find that for channels that exhibit a media layer height smaller than that of a neutrophil (~ 8-12 µm (*39*) at the channel entrance), cells get trapped by the media-oil interface at the entrance to the channel (**Fig 4C**). Furthermore, addition of FITC to the outlet droplet establishes a chemical gradient (**Fig 4D and E**). Taken together, these results suggest an ability to spatially control cell positioning using the rigidity of a liquid-liquid interface within open, physically accessible channels.

Neutrophil migration speed is dependent on the amount of required interfacial deformation to traverse through the channel

Given that the height of the media layer decays to zero at some point along the length of the channel, migration through the channel would require active deformation of the interface to allow space for migration, just as neutrophils deform cells to traverse between cell-cell junctions *in vivo*. Addition of the neutrophil chemoattractant N-Formylmethionine-leucyl-phenylalanine (fMLP, MW 437.56 g/mol) to the outlet droplet establishes a chemokine gradient relatively stable over experimental timescales of three hours

(**Supplementary Fig 2A**) and induces active neutrophil deformation and migration through the channel (**Fig 5A**). Throughout migration, two populations of cells arise. The initial cells to enter the channel, labeled “pioneer cells” migrate slowly, followed by “trailing” cells that migrate more rapidly through the channel (**Fig 5B and C**). Confocal imaging of migration reveals differential heights of the media layer before and after pioneer cell passage (**Fig 5D**), suggesting that active deformation of the channel interface facilitates passage. The interface is elastic, so that it can relax after leader cell passage (ex. point c in **Fig E**), however even with this relaxation, trailing cells are exposed to a significantly higher media height than pioneer cells thus require less interfacial deformation to allow passage.

There could be several mechanisms that lead to the differential migration speed between pioneer and trailing cells. One possible explanation of this disparity is alteration of the chemokine gradient by the physical deformations of the interface induced by pioneer cells. To investigate this, fluorescence intensity of FITC dye (similar molecular weight to fMLP; FITC 389.382 g/mol vs. fMLP 437.56 g/mol) was quantified at each point along the channel during cell migration to approximate the fMLP gradient over time (*40, 41*). Using this method, FITC partially labels pioneer cells to track their position over time (**Supplementary Fig 2B**). Notably, as pioneer cells move through the channel through time (position denoted by brackets), the gradient is neither spatially nor temporally altered (**Fig 5G**). Thus, to decouple chemical cues from physical changes in interface height, we analyzed a subset of trailing cells that migrate fast enough to catch up to and thus become pioneer cells faced with lower media layer height. These cells traverse the same positions as pioneer cells, yet significantly decrease in speed as they become pioneer cells (**Fig**

5H) suggesting a mechanism whereby channel height drives differential migration speed between pioneer and trailing cells.

Alternatively, pioneer cells themselves could secrete chemokines to alter migration speed of trailing cells, a known phenomenon termed swarming whereby neutrophils secrete a chemoattractant LTB4 to amplify migration speed of surrounding neutrophils. However, speed discrepancy between the two cell populations persisted even after inhibition of LTB4 production by the small molecule inhibitor MK866, suggesting a mechanism independent of LTB4-mediated signal relay (**Supplemental Fig 3C**). Additionally, migration speed of trailing cells does not continue to increase over the length of the channel as would be typical of swarming, but rather stays relatively constant (with even a slight decrease in speed) (**Supplemental Fig 3D**). Taken together, these data indicate a mechanical mechanism whereby pioneer cells actively deform the channel interface, leaving a higher media layer height to facilitate faster migration of trailing cells which require less interfacial deformation. Critically, these results demonstrate the ability to decouple chemical cues such as position within a gradient from mechanical cues of interfacial height to isolate the role of physical cues on cell phenotype.

Controlling interfacial pressure modulates neutrophil migration speed

Cells of different tissues exhibit a broad range of elastic moduli which alter the mechanical environment that neutrophils traverse *in vivo*. Nonetheless, how stiffness of a local deformable interface (i.e. a tissue-resident cell) mechanically interacting with neutrophils

affects cell migration is largely unexplored. To investigate this, we constructed two channels (30 µm width x 275 µm length and 100 µm width x 500 µm length) (**Fig 6A**) that generate similar chemical gradients (**Fig 6B**) yet allow for differential radii of curvature (**Fig 6C**) and thus pressures resisting deformation induced by migrating cells (**Fig 6D**). Media layer height of both channels decays to undetectable levels at comparable points along the channel length (**Fig 4C above**), requiring significant interfacial deformation by pioneer cells to facilitate migration. Migration on channels of lower interfacial pressure (100 µm width) migrate significantly faster than those on channels of high pressure (30 µm width). These data suggest that mechanical pressures resisting cell deformation of the interface influence neutrophil motility.

Interfacial deformation recapitulates surrounding single-cell epithelial deformations during neutrophil migration *in vivo*

Most all neutrophils migrating *in vivo* act as “pioneer” cells as they migrate between and deform surrounding cells (**Figure 7A**). Here, the *in vitro* liquid-liquid interface provides a deformable contact point to migrating neutrophils with comparable stiffness to individual cells (**Fig 7B**). Thus, to validate this system, we compared interfacial deformations induced by pioneer cells *in vitro* (**Fig 7C**) to those from neutrophils interacting with surrounding keratinocytes *in vivo* (**Fig 7D**). We find that mechanical deformations induced by pioneer cells are very similar to those of surrounding keratinocytes *in vivo* (**Fig 7E**). Given that our previous results suggest that the amount of required deformation influences migration speed, we also compared speeds between pioneer cells and *in vivo*

neutrophils. Where previous studies using rigid PDMS-based microchannels often report *in vitro* migration speeds significantly higher than those within *in vivo* models (*19*,*20*), migration speed of pioneer cells are similar to those observed *in vivo*. These data demonstrate the ability to model mechanical interactions between single leukocytes and surrounding keratinocytes *in vivo* using *in vitro* microchannels made of a liquid-liquid interface.

DISCUSSION

Here, we develop an *in vitro* system to study neutrophil migration under confinement in a more physiologically relevant environment. This addresses an important gap in the field because while it has become increasingly clear that local mechanical cues contribute to immune cell activation, cytokine production, metabolism, proliferation, and migratory capacity (*1-3*,*15-23*), further biological insights are constrained by our ability to model different mechanical cues present *in vivo*. While *in vivo* models have provided substantial breakthroughs in understanding how leukocytes traverse tissues to sites of inflammation, isolating and controlling local mechanical cues surrounding individual cells is difficult if not impossible. *In vitro* methods that utilize hydrogels provide some control by tuning gels to a bulk stiffness, or average pore and fiber size. PDMS-based microfluidic channels provide a high degree of control over cell confinement. However, the vast majority of tissue volume is resident cells (especially in non-fibrotic, healthy tissue), that are soft and mechanically interact with migrating cells, interactions absent from current *in vitro* systems.

Recently there has been substantial interest in the migration of leukocytes under mechanical confinement *in vitro*. Interestingly, progressive neutrophil confinement within PDMS-microchannels has been shown to increase migration speed up a chemokine gradient (*19*) yet also induce retrotaxis, or movement away from an attractive chemokine (*45*). Critically intertwined with cell migration is polarity, the ability for a cell to establish a leading front and a trailing edge. Recently, mechanical confinement of cells has revealed a novel cell polarity program under inhibition of canonical polarity machinery (*46*). Distinct from confinement alone, microchannels have been used to study how other physical cues (i.e. hydraulic pressure) (*47,48*) or breakdown of chemical cues (*49*) effects cell decision making regarding directionality. Here, we characterize reciprocal mechanical interactions between migrating neutrophils and surrounding cells within an *in vivo* model and construct *in vitro* microchannels to replicate this mechanical interaction. Through this, we identify that the amount of required deformation of a confining elastic interface regulates migratory capacity of neutrophils. We find that controlling pressures resisting deformation of the channel interface modulates migration speed. The ability to model novel mechanical interactions between a migrating cell and the local environment *in vitro* provides an intriguing avenue for future discoveries on how mechanical cues regulate cell migration biology.

One future application is in understanding how the varying cellular mechanical properties between different tissue types impacts immune cell recruitment. Our data would suggest that neutrophils surrounded by stiffer interfaces (ex. cells of the skin) might

migrate slower than those navigating through an environment of more fluidic cells (ex. within the lungs). Furthermore, mechanical properties also change throughout time in the context of disease (i.e cancer, autoimmune disease) or tissue injury. For example, proper tissue healing following injury is reliant on precise coordination of leukocyte recruitment and later egress from sites of inflammation. Tissue mechanical properties change over the course of injury through transient cell apoptosis and swelling then progressive fibrosis and cell stiffening. As we have come to better appreciate the role of external mechanical cues in regulating the immune response, it is possible that the changes in tissue mechanical properties during wounding are not only the effect of an initial insult but may be a well-coordinated driver in regulating the subsequent immune response. A challenge in approaching this question, and a limitation of this study, is difficulty in characterizing mechanical properties of *in vivo* tissues on near single cell length scales. Precise mapping of tissue mechanical properties between different tissues and disease states within *in vivo* systems might reveal how mechanical properties of surrounding cells impacts immune cell recruitment. In parallel, the controllability of novel *in vitro* models as introduced here might identify how mechanical interactions with similar interfaces are transduced into intracellular chemical signals to alter cell phenotype.

METHODS

Whole blood collection

All blood samples were drawn according to Institutional Review Boards (IRB) approved protocols per the Declaration of Helsinki at the University of Wisconsin-Madison in the Beebe Lab (IRB# 2020 − 1623) and in the Huttenlocher Lab (IRB#, 2017-003). Informed consent was obtained from all subjects in the study. Whole blood was collected with standard ethylenediaminetetraacetic acid (EDTA) tubes (BD, #36643, EDTA [K2] STERILE, 1054688) and then stored at RT (~ 22 °C) or 37 °C in stationary storage before isolation.

Neutrophil isolation and culture

Neutrophils were isolated from whole blood using magnetic bead-based negative selection per protocol using the EasySep Direct Human Neutrophil Isolation Kit (STEMCELL, 19666). After isolation, the neutrophil pellet was directly resuspended in appropriate media for further experiments. Cell count of each isolation was obtained using a hemocytometer (LW Scientific). Following resuspension, liquid cultures were stored at 37° in a standard CO2 incubator (Thermo Scientific, HERACELL 240i) for no more than 1 hour before transfer to an onstage incubator (Bold Line, Okolab) for imaging in an experiment.

Device Construction

A premium microscope slide (Fisherfinest, 3″ × 1″ × 1 mm; Thermo Fisher Scientific, 12-544-1) or chambered coverglass (1 well, no. 1.5 borosilicate glass, 0.13 to 0.17 mm thick;

Thermo Fisher Scientific, 155360) was treated first with O2 plasma (Diener Electronic Femto, Plasma Surface Technology) at 60 W for 3 min and then moved to an oven for grafting of PDMS-Silane (1,3-dichlorotetramethylsiloxane; Gelest, SID3372.0) (about 10 µl per device) onto the glass surface by chemical vapor deposition (CVD).

The PDMS-grafted slide was masked by a PDMS stamp (stamp construction described in *29*) and treated with O_2 plasma at 60 W for 3 min. After surface patterning, the PDMS stamp was removed by tweezers and stored in a clean space for reuse. The glass slides were held in a plate [Nunc four-well tray, polystyrene (PS), non-treated sterile, Thermo Fisher Scientific, 267061] and overlaid with oil (silicone oil, 5 cSt; Sigma-Aldrich, 317667). The chambered coverglass was directly overlaid with oil.

ECM gel preparation

One part rat tail collagen I (Corning, 10 mg/mL)) was neutralized with one part neutrophil culture media (Roswell Park Memorial Institute (RPMI) 1640 Medium, Thermo Fisher Scientific,11875093) + 10% fetal bovine serum (Thermo Fisher Scientific, 10437010) and one part 2X HEPES buffer. One in 16 parts RFP-labeled rat tail collagen was added to allow for imaging of fibers, yielding a final concentration 3.125 mg/mL of rat tail collagen. The pH of the collagen mixture was adjusted to pH 7.2 before being used to construct channels. Channels were constructed by sweeping hanging droplets of collagen solution +/- cells across O2-plasma patterned areas.

Quantification of hell heights and capillary pressures

To quantify cell heights and corresponding capillary pressures at locations of cells passively placed into channels of varying heights, sweep was performed with a suspension of cells in collagen mixture at a final concentration of ~ 30 cells/uL. Immediately after sweep, channels were incubated at 37° for 20 minutes to facilitate collagen polymerization. Channel and cell heights were quantified in FIJI from confocal z-stacks taken at .2 µm slice intervals at room temperature on a Nikon Ti2 spinning disk confocal microscope (Nikon Instruments) within the UW-Madison Optical Core. Capillary pressure of channels without cells was calculated by manually drawing circles around channels in the cross-sectional plane to estimate radius of curvature. A parallel method was used to estimate pressures around locations of cells to estimate radii of curvature in both relevant planes (cross-sectional and side views).

Cell trapping and gradient quantification

Channels were made of collagen as above then 1 µL of primary neutrophils at 20k/µL concentration was added to the inlet droplet by pipetting. FITC was added to culture media at 25 µM and confocal imaging performed to quantify profiles of the media height layer for different channels. To estimate fMLP gradients across the length of the channel, FITC (25 µM) was added to outlet droplets of collagen channels and imaged on a Nikon Ti Eclipse inverted epifluorescence microscope (Nikon Instruments). Fluorescent intensity at points along the channel was quantified in FIJI. Gradient profiles were captured at various times, each time normalizing for maximum intensity at the center of the outlet droplet. To estimate gradients of fMLP, the maximum intensity of FITC at the center of the outlet droplet was mapped to the known concentration added into the outlet

droplet (100 nM fMLP) with linear mapping of subsequent intensity values to a corresponding FITC concentration. Gradient estimation during cell migration was done using an equivalent method.

Quantification of migration speed and interfacial deformations

Cells were added to the inlet droplet of collagen channels at concentration 20k cells/µL and 1 µL of 100 nM fMLP added to the outlet droplet. The channels were kept at 37 oC, 21% or 5% O2, 5% CO2, and 95% RH in an onstage incubator (Bold Line, Okolab) during the time lapse imaging (brightfield, 30 sec time intervals) on the Nikon fluorescent scope noted above. Manual cell tracking was performed in FIJI using the manual tracking plug-in. An identical experimental set up was performed to quantify channel media layer height and interfacial deformations during migration however imaging performed on a spinning disk confocal microscope (Nikon Ti2 noted above). Images of multiple different channels (n = 12) was obtained at various time points throughout migration to quantify average channel height before and after pioneer cells and thus required deformation of pioneer cells.

Zebrafish maintenance and handling

Animal care and use was approved by the Institutional Animal Care and Use Committee of University of Wisconsin and strictly followed guidelines set by the federal Health Research Extension Act and the Public Health Service Policy on the Humane Care and

Use of Laboratory Animal, administered by the National Institutes of Health Office of Laboratory Animal Welfare. All protocols using zebrafish in this study were approved by the University of Wisconsin-Madison Research Animals Resource Center (protocol M005405-A02). Previously published transgenic lines *Mpx:mCherry* (Yoo et al., 2010) and *Krtt1c19e:acGFP (Gift of Dr. Alvaro Sagasti)* were maintained on the AB background. Following breeding, fertilized embryos were transferred to E3 medium (5 mM NaCl, 0.17 mM KCl, 0.44 mM $CaCl_2$, 0.33 mM $MgSO_4$, 0.025 mM NaOH, and 0.0003% Methylene Blue) and maintained at 28.5°C. Larval zebrafish were anesthetized using 0.2 mg/ml tricaine (ethyl 3-aminobenzoate; Sigma-Aldrich) before any experimentation or live imaging.

Tracking in-vivo keratinocyte deformations

Dechorionated, tricaine-anesthetized 3 or 4 days-post fertilization (dpf) larvae were mounted in 2% low-melting point agarose (Sigma-Aldrich) on a 35 mm glass bottom dish (#1.5H Glass, Cellvis, CA, USA). Time-lapse imaging of neutrophil migration through basal keratinocytes in the yolk sac was performed on an spinning-disk confocal (CSU-X; Yokogawa) on a Zeiss Observer Z.1 inverted microscope and an electron-multiplying charge-coupled device Evolve 512 camera (Photometrics), with a EC Plan-Neofluar 40×/NA 0.75 air objective (1-2µm optical sections, 2,355 × 512 resolution) using ZenPro 2012 software (Zeiss).

Statistical Analysis

Data were analyzed (Prism 9.0; GraphPad Software). Statistical significance was assessed using Student's *t* tests when comparing two conditions/groups, and when comparing more than two groups, significance was assessed using one-way analysis of variance (ANOVA) corrected using the Tukey's test.

FIGURES

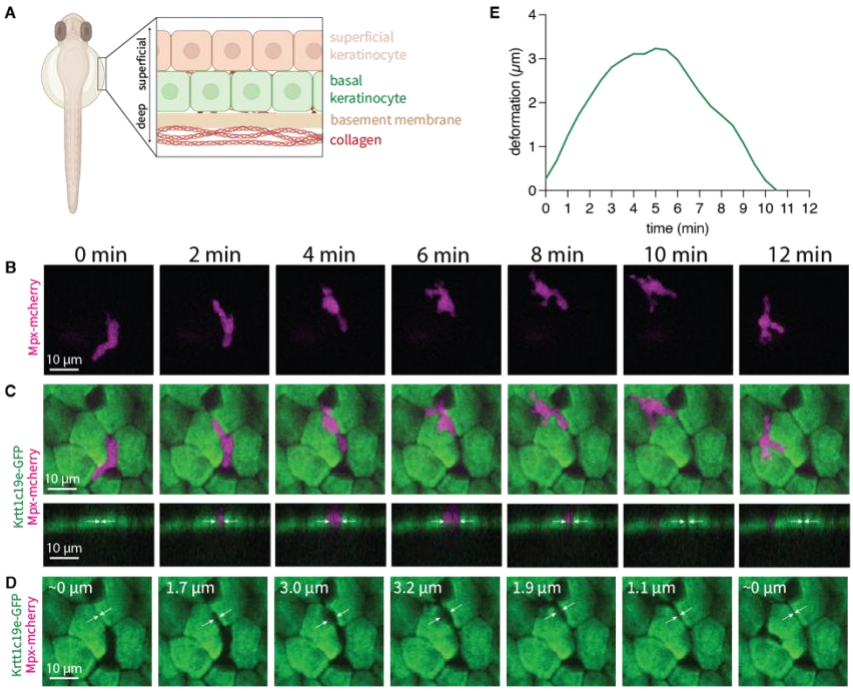

Fig. 1 Neutrophils mechanically interact with resident basal keratinocytes during migration in zebrafish. A) Schematic of 3 day post fertilization (dpf) zebrafish skin. The basal keratinocytes represent a single-cell thick layer immediately beneath the superficial keratinocytes supported by a basement membrane. **B)** Time-lapse images of migrating neutrophils within the skin of the yolk sac show characteristic dynamics in cell morphology during migration. **C)** Visualization of basal keratinocytes reveals an influence of surrounding cells that mechanically confine migrating neutrophils. **D)** Neutrophils mechanically interact with and deform keratinocytes during migration. **E)** Representative quantification of keratinocyte deformation over time.

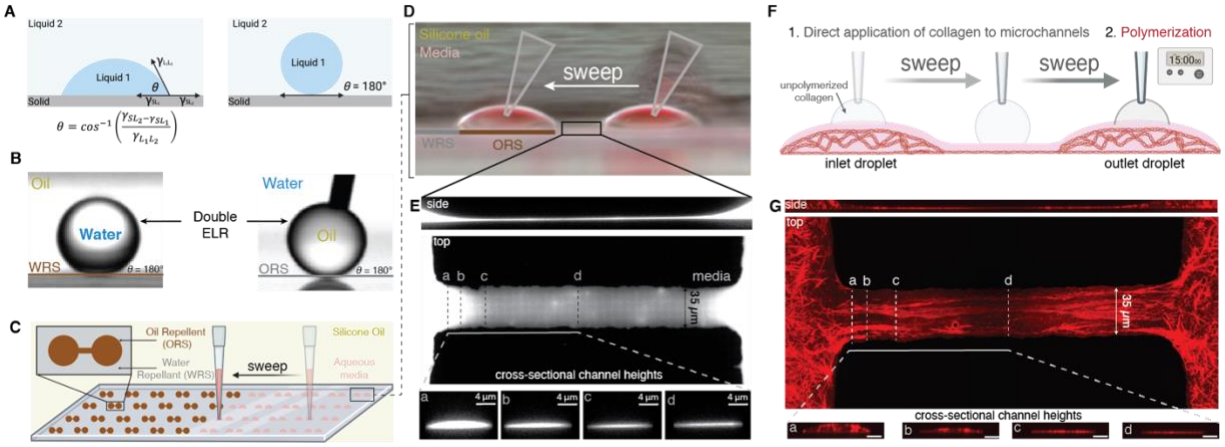

Fig. 2 Construction of fibrillar collagen coated liquid-liquid microchannels enabled by double ELR. A) The inherent liquid repellency of a surface is characterized by Young's contact angle, determined by the balance of interfacial energies (γ_{SL1}, γ_{SL2}, γ_{L1L2}) between all phases of the system (ex. solid-liquid-liquid). An ELR surface completely repels one liquid when in the presence of another, resulting in a Young's contact angle of 180°. **B)** Double ELR refers to a system whereby a surface is differentially patterned with areas that are ELR to water in the presence of a third oil phase (Water Repellent Surface, WRS) or ELR to oil in the presence of a third water phase (Oil Repellent Surface, ORS). **C)** Engineering a double ELR system by selective chemical patterning of both ORS and WRS areas allows construction of liquid channels by "sweeping" aqueous media across ORS regions. **D)** Macroscale side view of a channel, characterized by two droplets connected by a liquid bridge. **E)** A representative channel of 30 µm width and < 2 µm height. The channel height tapers at the entrance to a relatively consistent height (points c-d) until a gradual height increase towards the channel exit. **F)** The open nature of the platform allows incorporation of fibrillar collagen into channels by direct physical addition

through the “sweep” technique. (**G**) Representative confocal image of 35 µm width collagen channel. The scale bar in cross-sectional images represents 6 µm.

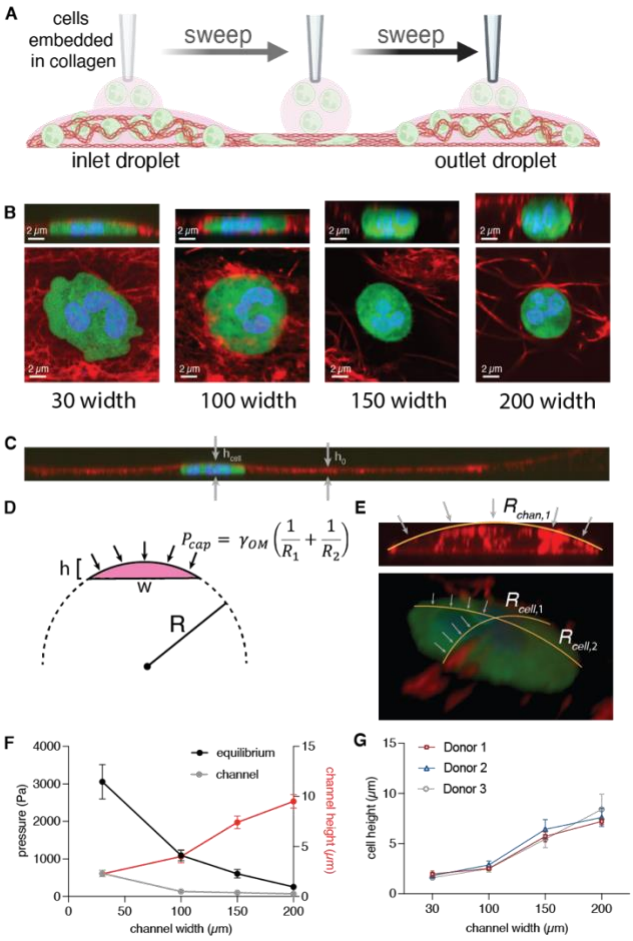

Fig. 3 Interfacial pressure of liquid-liquid microchannels confine neutrophils A) Sweeping channels with cells embedded in neutralized collagen solution deposits cells into the channel, subjecting them to confinement by the liquid-liquid interface. **B)** Neutrophils placed within channels of varying size (width 200 µm to 30 µm) and thus height exhibit differential degrees of cell confinement. **C)** The presence of cells locally deforms the channel interface so that an interface of initial height h_0 becomes deformed in the presence of a cell to a height h_{cell}. **D)** Capillary pressure resisting interfacial deformation arises from the presence of curvature and is a given by the LaPlace equation.

Pressure is a function of the oil-media interfacial energy (41.8 mN/m) and the radii of curvature (R) present within the system. **E)** In the absence of cells, channels exhibit curvature only along the width of the channel (curvature along channel length is infinite) resulting in an initial channel pressure P_{chan}.= γ_{OM}/R. Channel deformation by cells results in curvature over both the length and width of the cell resulting in two radii of curvature and an equilibrium pressure $P_{chan} = \gamma_{OM}/(R_{cell,1} + R_{cell,2})$. **F)** Channel pressures (gray) and equilibrium pressures in the presence of cells (black) for varying channel widths. Channel height (red) increases with channel width. Channel pressure and height was calculated from three independent replicates from each channel width. **G)** The height of confined cells (taken from three independent donors) thus increases with channel width.

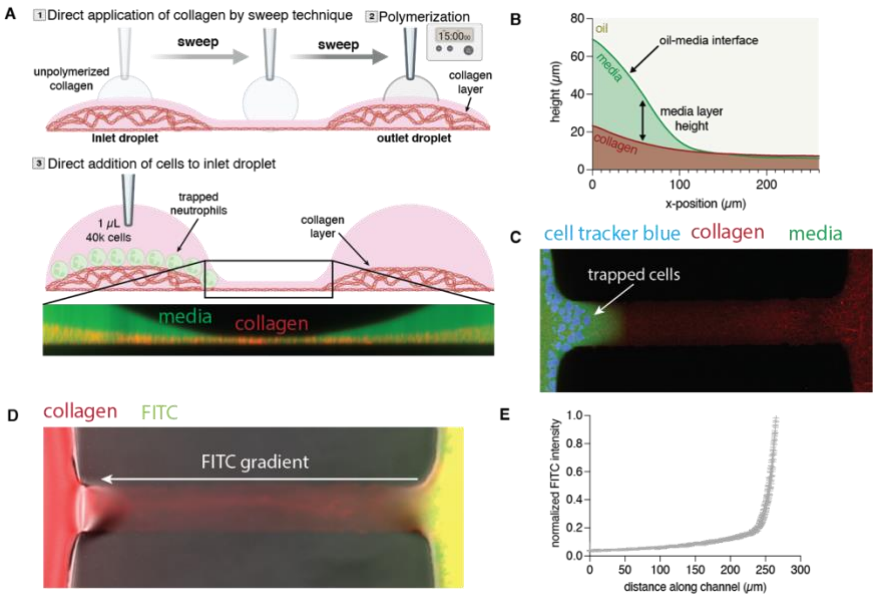

Fig. 4 Open-fluid cell trapping and establishment of a chemical gradient along a collagen substrate. A) Open access allows direct addition of collagen. Sequential addition of media creates a media layer on top of a layer of polymerized collagen. **B)** Representative plot of media and collagen layers for a 200 µm width channel. **C)** Representative image of cell trapping at the entrance to a 30 µm width (~ 2 µm height)

channel. **D)** Addition of FITC atop polymerized collagen to the outlet droplet allows the establishment of a gradient. **E)** FITC gradient over three independent replicates quantified by fluorescence intensity along the channel length, normalized to maximum intensity at the center of the outlet droplet.

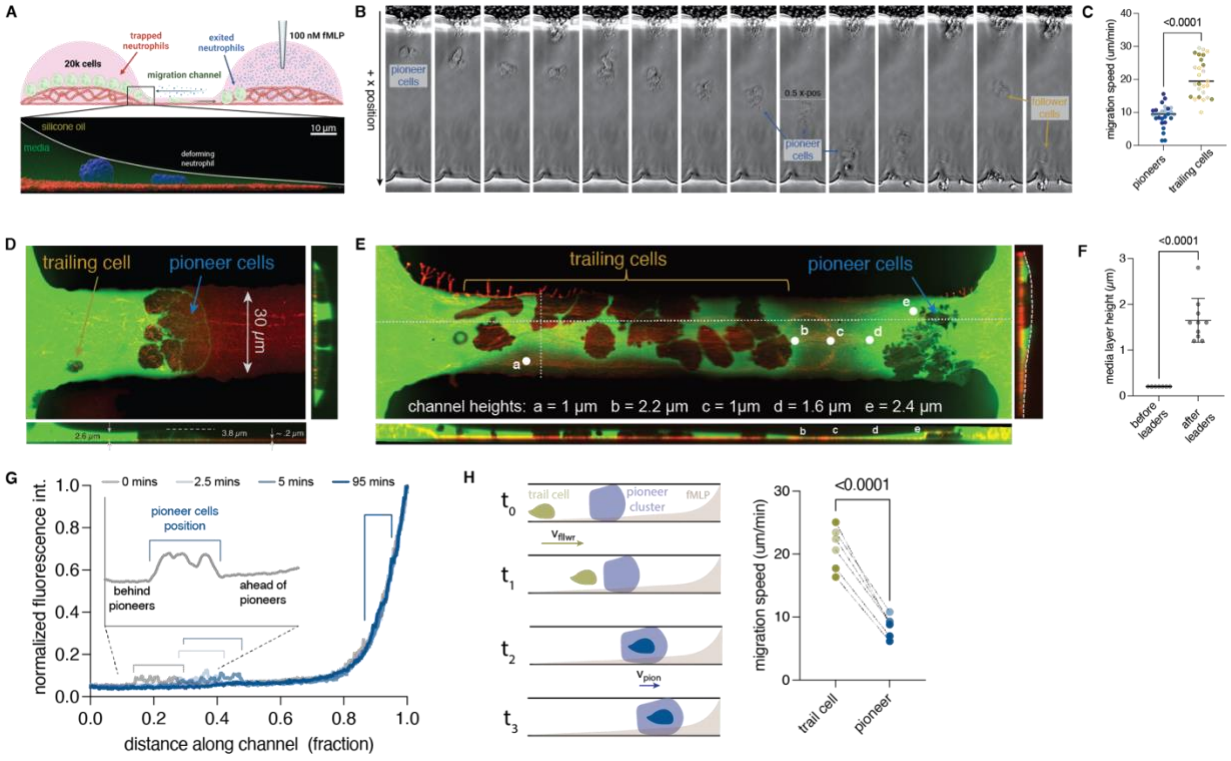

Fig. 5 Neutrophil migration speed is dependent on required interfacial deformation. A) Addition of chemokine opposite from cells triggers active cell deformation captured by a confocal reconstruction within Imaris. **B)** Two distinct populations of cells emerge during migration. The first cells to contact the interface of the channel (pioneer cells) migrate slowly, followed by trailing cells that migrate more rapidly through the channel. **C**) Plot of migration speed of pioneer and trailing cells for three different donors (pioneer/trailing cell pairs chosen over the same three replicates for each donor). Each point represents the

speed of a single cell. **D)** Pioneer cells deform the interface to increase the interfacial height preceding trailing cells. **E)** The interface is elastic, so that it relaxes (ex. point c) after pioneer cell passage. **F)** However, even accounting for elastic relaxation, pioneer cells are subjected to a significantly lower interfacial height compared to trailing cells and thus require greater deformation to facilitate migration. Each point represents a single cell taken over three independent replicates from the same donor. **G)** Pioneer cell migration does not significantly alter the chemical gradient, determined by fluorescence intensity of FITC dye added to the outlet droplet. The location of pioneer cells is evident from peaks in fluorescent intensity due to faint cell labeling with FITC and denoted by brackets over time. **H)** Schematic and corresponding plot of neutrophils that start as trailing cells that catch up to and become leader cells over time. Each data point represents a cell (taken from an independent channel) and shade represents donor. Significance for all comparison was determined by a two-sample independent t-test assuming equal variances.

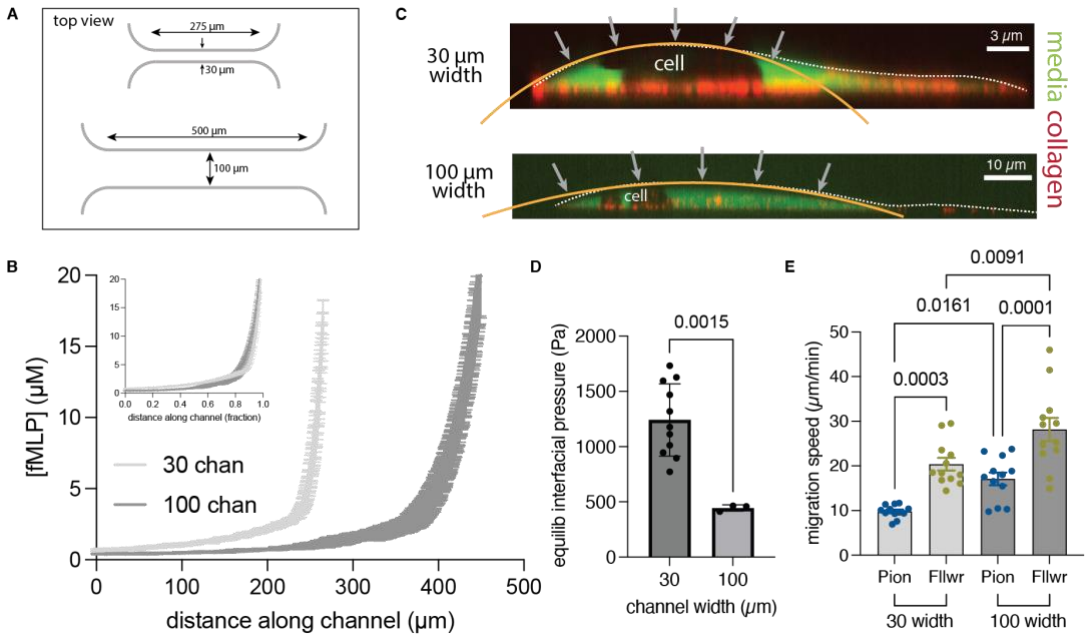

Fig. 6 Neutrophil migration speed is dependent on pressure resisting deformation. **A)** Schematic of channel geometries. **B)** These channels generate similar chemical gradients, with the larger channel producing a slightly steeper gradient. Data was generated from three independent channel replicates. **C)** Representative images of migrating cells exposed to differential pressures resisting deformation. **D)** Quantification of equilibrium pressures. Each data point represents a single cell from three replicates from a single donor. Statistical significance was determined by a two-sample independent t-test assuming equal variances. **E)** Neutrophils on both channels exhibit pioneer (Pion)-follower (Fllwr) phenotypes, however cells on channels of lower pressure exhibit faster migration speeds. Each data point represents a single cell from a single donor, pooled over three separate replicates. Significance was determined by a one-way ANOVA with multiple comparisons assuming equal variances.

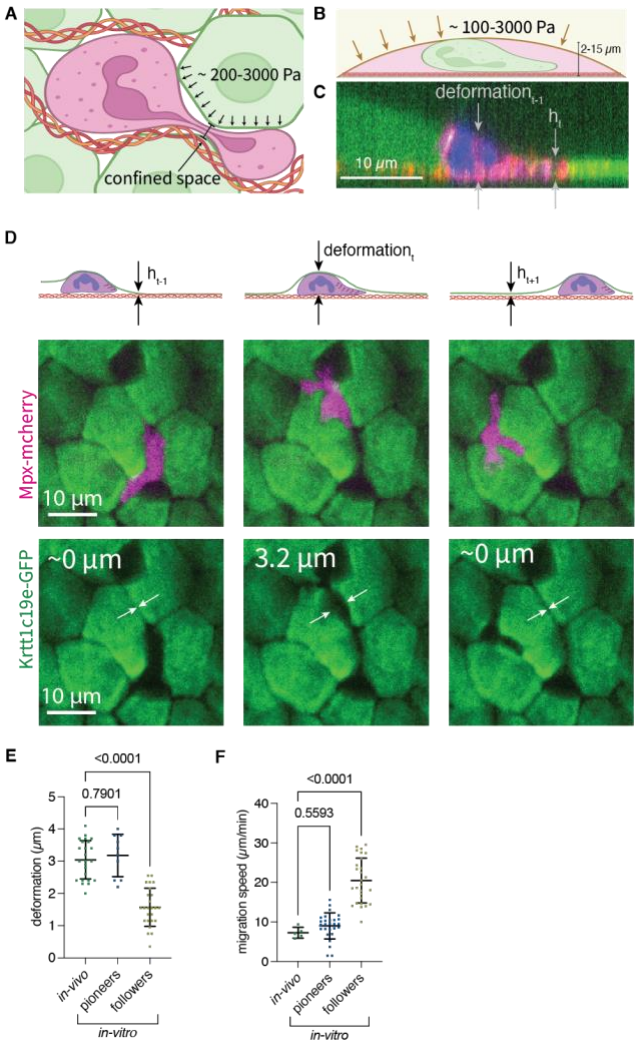

Fig. 7 Interfacial deformation recapitulates surrounding single-cell epithelial deformations during neutrophil migration *in vivo*. A) Schematic of neutrophil migration along ECM proteins between tissue-resident cells. **B)** Schematic of confined neutrophil migration along a collagen substrate in liquid-liquid channels. **C)** Representative interfacial height during deformation by a pioneer cell. **D)** Interfacial deformations during pioneer cell migration on a 30 µm width channel were compared to those exhibited by keratinocytes *in vivo.* **E)** Interfacial deformations induced by pioneer cell migration replicate those of surrounding keratinocytes during *in vivo* migration. **F)**

Pioneer cells replicate migration speed of neutrophils traversing between keratinocytes *in vivo*. Each data point is a single cell taken for three donors (3 replicates each), or three fish. Statistical significance was determined by a one-way ANOVA with multiple comparisons to the *in vivo* group assuming equal variances.

REFERENCES

1. M. Huse, Mechanical forces in the immune system. Nat Rev Immunol 17, 679-690 (2017).

2. C. Zhu, W. Chen, J. Lou, W. Rittase, K. Li, Mechanosensing through immunoreceptors. Nat Immunol 20, 1269-1278 (2019).

3. S. van Helvert, C. Storm, P. Friedl, Mechanoreciprocity in cell migration. Nat Cell Biology 20, 8-20 (2018)

4. S. de Oliveira, E. Rosowski, A. Huttenlocher, Neutrophil migration in infection and wound repair: going forward in reverse. Nat Rev Immunol 16, 378–391 (2016).

5. T. Lammermann et al., Neutrophil swarms require LTB4 and integrins at sites of cell death in vivo. Nature 498, 371-375 (2013).

6. K. Kienle et al., Neutrophils self-limit swarming to contain bacterial growth in vivo. Science 372, eabe7729 (2021).

7. S. K. Yoo et al., Differential regulation of protrusion and polarity by PI3K during neutrophil motility in live zebrafish. Dev Cell 18, 226-236 (2010).

8. F. Barros-Becker, P. Y. Lam, R. Fisher, A. Huttenlocher, Live imaging reveals distinct modes of neutrophil and macrophage migration within interstitial tissues. J Cell Sci 130, 3801-3808 (2017).

9. K. Siemsen et al., Tunable 3D Hydrogel Microchannel Networks to Study Confined Mammalian Cell Migration. Adv Healthc Mater 10, e2100625 (2021).

10. J. FranÁois et al., The interplay between matrix deformation and the coordination of turning events governs directed neutrophil migration in 3D matrices. Science Advances 7, eabf3882 (2021).

11. C.F Guimarães, L. Gasperini, A.P. Marques, et al. The stiffness of living tissues and its implications for tissue engineering. Nat Rev Mater 5, 351–370 (2020).

12. A.K. Denison and B.L. Pruitt. Tuning the Range of Polyacrylamide Gel Stiffness for Mechanobiology Applications. ACS Applied Materials & Interfaces *8* (34), 21893-21902 (2016).

13. K.A Ross, M.G Scanlon. Analysis of the elastic modulus of agar gel by indentation. Journal of Texture Studies 30, 17-27 (1999)

14. R. Seghir and S. Arscott. Extended PDMS stiffness range for flexible systems. Sensors and Actuators A: Physical 230, 33-39 (2015).

15. N. Wang, E. Ostuni, G. M. Whitesides, D. E. Ingber, Micropatterning tractional forces in living cells. Cell Motil Cytoskeleton 52, 97-106 (2002).

16. F. Wang, P. Herzmark, O Weiner, et al. Lipid products of PI(3)Ks maintain persistent cell polarity and directed motility in neutrophils. Nat Cell Biol 4, 513–518 (2002).

17. T. Y. Tsai et al., Efficient Front-Rear Coupling in Neutrophil Chemotaxis by Dynamic Myosin II Localization. Dev Cell 49, 189-205.e186 (2019).

18. R. T. Tranquillo, S. H. Zigmond, D. A. Lauffenburger, Measurement of the chemotaxis coefficient for human neutrophils in the under-agarose migration assay. Cell Motil Cytoskeleton 11, 1-15 (1988).

19. L. Boneschansker, J. Yan, E. Wong, et al. Microfluidic platform for the quantitative analysis of leukocyte migration signatures. Nat Commun 5, 4787 (2014).

20. B. Hamza et al., Retrotaxis of human neutrophils during mechanical confinement inside microfluidic channels. Integr Biol (Camb) 6, 175-183 (2014).

21. YJ. Liu, M. Le Berre, F. Lautenschlaeger, et al. Confinement and low adhesion induce fast amoeboid migration of slow mesenchymal cells. Cell 4, 659-672 (2015).

22. P. W. Kriebel, V. A. Barr, E. C. Rericha, G. Zhang, C. A. Parent, Collective cell migration requires vesicular trafficking for chemoattractant delivery at the trailing edge. J Cell Biol 183, 949-961 (2008).

23. S. B. Arya, S. Chen, F. Jordan-Javed, C. A. Parent, Ceramide-rich microdomains facilitate nuclear envelope budding for non-conventional exosome formation. Nat Cell Biol 24, 1019-1028 (2022).

24. T.F. Robertson and A. Huttenlocher. Real-time imaging of inflammation and its resolution: It's apparent because it's transparent. Immunol Rev. 306 (1), 258-270 (2022).

25. C. Li, Y. Jiaquan, S. Jennifer, et al. Exclusive Liquid Repellency: An Open Multi-Liquid-Phase Technology for Rare Cell Culture and Single-Cell Processing. ACS Applied Materials & Interfaces 10 (20), 17065-17070 (2018)

26. C. Li, Y Jiaquan, P Paine, et al. Double-exclusive liquid repellency (double-ELR): an enabling technology for rare phenotype analysis. Lab on Chip 18, 2710-2719 (2018)

27. E. J. Walsh et al., Microfluidics with fluid walls. Nat Commun 8, 816 (2017).

28. C. Deroy, , A.N. Rumianek, J.H.R Wheeler, et al. Assaying Macrophage Chemotaxis Using Fluid-Walled Microfluidics. Adv. Mater. Technol. 7, 2200279 (2022)

29. C. Deroy et al., Predicting flows through microfluidic circuits with fluid walls. Microsyst Nanoeng 7, 93 (2021).

30. W. Feng et al., Harnessing liquid-in-liquid printing and micropatterned substrates to fabricate 3-dimensional all-liquid fluidic devices. Nat Commun 10, 1095 (2019).

31. C. Li et al., Under oil open-channel microfluidics empowered by exclusive liquid repellency. Sci Adv 6, eaay9919 (2020).

32. S. I. Fraley et al., Three-dimensional matrix fiber alignment modulates cell migration and MT1-MMP utility by spatially and temporally directing protrusions. Sci Rep 5, 14580 (2015).

33. P.P. Provenzano, K.W. Eliceiri, J.M. Campbell, et al. Collagen reorganization at the tumor-stromal interface facilitates local invasion. BMC Med 4, 38 (2006).

34. K. M. Yamada, M. Sixt, Mechanisms of 3D cell migration. Nat Rev Mol Cell Biol 20, 738-752 (2019).

35. S. SenGupta, C. A. Parent, J. E. Bear, The principles of directed cell migration. Nat Rev Mol Cell Biol 22, 529-547 (2021).

36. Z. Zhou, F. Cui, Q. Wen, H. Susan Zhou, Effect of vimentin on cell migration in collagen-coated microchannels: A mimetic physiological confined environment. Biomicrofluidics 15, 034105 (2021).

37. B. Burkel et al., Preparation of 3D Collagen Gels and Microchannels for the Study of 3D Interactions In Vivo. J Vis Exp, (2016).

38. X. Wang, L. Zhaomiao, Y. Pang. Concentration gradient generation methods based on microfluidic systems. RSC Adv 7, 29966-29984 (2017)

39. H. Somaweera, A. Ibraguimov, D. Pappas, A review of chemical gradient systems for cell analysis. Anal Chim Acta 907, 7-17 (2016).

40. V. Abhyankar, M.A. Lokuta, A. Huttenlocher, D.J. Beebe. Characterization of a membrane-based gradient generator for use in cell-signaling studies. Lab on Chip 6, 389-393 (2006)

41. P. X. Liew, P. Kubes, The Neutrophil's Role During Health and Disease. Physiological Reviews 99, 1223-1248 (2019).

42. H. Cho, B. Hamza, E.A. Wong, D. Irimia. On-demand, competing gradient arrays for neutrophil chemotaxis. Lab Chip. 14 (5), 972-978 (2014)

43. A. Chandrasekaran, F. Ellett, J. Jorgensen, D. Irimia. Temporal gradients limit the accumulation of neutrophils toward sources of chemoattractant. Microsyst Nanoeng 3, 16067 (2017)

44. M. Januszyk, V.W. Wong, K.A. Bhatt, et al. Mechanical offloading of incisional wounds is associated with transcriptional downregulation of inflammatory pathways in a large animal model. Organogenesis 10 (2), 186-193 (2014)

45. X. Wang, E. Jodin, J Jorgenson, et al.Progressive mechanical confinement of chemotactic neutrophils induces arrest, oscillations, and retrotaxis. J Leukoc Biol. 104 (6), 1253-1261 (2018).

46. B.R. Graziano, J.P. Town, E. Sitarska, et al. Cell confinement reveals a branched-actin independent circuit for neutrophil polarity. PLoS Biol. 17 (10), e3000457 (2019).

47. H.V. Prentice-Mott, C.H. Chang, L. Mahadevan, et al. Biased migration of confined neutrophil-like cells in asymmetric hydraulic environments. Proc Natl Acad Sci 110 (52), 21006-11 (2013).

48. J. Renkawitz, A Kopf, J Stopp, et al. Nuclear positioning facilitates amoeboid migration along the path of least resistance. Nature 568 (7753), 546-550 (2019).

49. L.Tweedy, P.A. Thomason, P.I. Paschke, et al. Seeing around corners: Cells solve mazes and respond at a distance using attractant breakdown. Science 369, eaay9792 (2020).